DOE/ER/60764--2

DE91 001666

DOE/ER/60764-2

RESEARCH IN RADIOBIOLOGY

Annual Report of Work in Progress in
Cell Specific Radiation Dosimetry in the
Skeleton from Lifespan Carcinogenesis Studies

RADIOBIOLOGY DIVISION
UNIVERSITY OF UTAH SCHOOL OF MEDICINE

JULY 15, 1990

U. S. DEPARTMENT OF ENERGY
GRANT DE-FG02-89ER60764

Technical Progress During the Past Year.

We have made good progress toward several of our specific aims. The details are given under "Accomplishments". These activities are summarized below:

A. Bone cells at risk. We have completed one experiment with the rat cortical bone remodeling model system and found the model will allow us to trace the appearance of preosteoblasts near bone surfaces, to determine whether the bone-lining cell is the terminal differentiation of osteoblasts, to label bone-lining cells and do experiments to trace its fate. The type, number and labeling indices of bone cells residing near bone-forming surfaces are being determined.

B. Bone cell morphometry. In the same rat cortical bone remodeling model system, we are characterizing the bone cells residing within the range of the bone-seeking radionuclide deposited on bone surface.

C. Bone cell residence time. The bone turnover rates and the morphometry of six cancellous and six cortical bone sites in the Beagle and St. Bernard dogs have been determined. The impact upon bone turnover by increasing body weight in a large dog, like a St. Bernard, and by underloading and overloading rat cancellous bones were also studied. Determining the turnover rates will allow us to calculate bone cell residence times for select bones.

D. Microdistribution of ^{239}Pu. A major breakthrough was made in this task. We developed "A Method to Analyze Neutron-induced Autoradiographs (NIAR), from ^{239}Pu Contaminated Bone Sections". This is a semi-automated system that reduces the tedium of counting fission tracks. This system automated the accumulation and analysis of numerous measurements. The information will allow us to develop models of the kinetics of ^{239}Pu using actual data, when formerly it was hypothesized.

The microscopic distribution of ^{239}Pu of five bone sites from 15 serially sacrificed confined dogs has been completed.

E. Calculation of cell-specific radiation dosimetry. There have been two manuscripts generated from this task: 1) one on the calculation of hit frequencies to bone-lining cells from alpha-emitting radionuclides using a Monte Carlo procedure; and 2) one on the prediction of tumor risk site from collective dose to either bone-lining cells or osteoblasts. The former is of importance with regard to tumor induction and cell-specific hit frequencies that will be calculated from our data. The latter article reiterates the need for more static and dynamic morphometry data on the Beagle skeleton and for better data on the microdistribution of ^{239}Pu (improve Pu affinity ratios of trabecular to cortical surface, forming and resting surfaces, etc.).

B. Bibliography of publications emanating from this project:

1) Polig, E., Jee, W.S.S., Johnson, F. and Dell, R.B. 1988. Microdistribution and local dosimetry of ^{226}Ra in trabecular bone of the beagle. Radiat. Res. 116:263-282.
2) Jee, W.S.S., Miller, S.C., Li, X.J., and DeSalva, S. 1988. Effects of N,N,N^1,N^1-ethylenediamine tetramethylene phosphonic acid on cortical bone remodeling in the adult dog. Toxicol. Appl. Pharmacol. 92:335-342.
3) Schaffler, M.B., Li., X.J., Jee, W.S.S., Ho, S.W.W., and Stern, P.J. 1988. Skeletal tissue responses to thermal injury: An experimental study. Bone 9:397-406.
4) Jee, W.S.S., Li, X.J., and Li, Y.L. 1988. Flurbiprofen-induced stimulation of periosteal bone formation and inhibition of bone loss in older rats. Bone. 9:381-389.
5) Li., X.F., Jee, W.S.S., and Li, Y.L. 1989. Flurbiprofen enhances growth and cancellous and cortical bone accumulation in rapidly growing long bones. Bone 10:35-44.
6) Li, X.F., Dawson-Hughes, B., Hopkins, R., Russell, R.M., Jee, W.S.S., Bankson, D., and Li, X.J. 1989. The effects of chronic vitamin A excess on bone remodeling in aged rats. Proc. Exptl. Biol. & Med. 191:103-107.
7) Polig, E., and Jee, W.S.S. 1989. Bone structural parameters, dosimetry, and relative radiation risk in beagle skeleton. Radiat. Res. 120:83-101.
8) Polig, E., and Jee, W.S.S. 1989. Microdistribution of radium-226 in the beagle skeleton and the resulting radiation dose to the target cell. Brit. Inst. Radiology Report, 21:77-81.
9) de Saint Georges, L., Miller, S.C., Bowman, B.M., and Jee, W.S.S. 1989. Ultrastructural features of osteoclasts in situ. Scanning Microscopy, 3:963-970.
10) Miller, S.C., de Saint-Georges, L., Bowman, M., and Jee, W.S.S. 1989. Bone-lining cells: Structure and function. Scanning Microscopy, 3:953-961.
11) Polig, E., and Jee, W.S.S. A model of osteon closure in cortical bone. Calcif. Tissue Int. (in press).
12) Li, X.J., Jee, W.S.S., Chow, S.Y., and Woodbury, D.M. 1990. Adaptation of cancellous bone to aging and immobilization in the rat: A single photon absorptiometry and histomorphometry study. Anat. Rec.227:12-24.
13) Jee, W.S.S., and Li, X.J. Adaptation of cancellous bone to overloading in the adult rat: a single photon absorptiometry and histomorphometry study. Anat. Rec. (in press).
14) Mori, S., Jee, W.S.S., Li, X.J., Chan, S., and Kimmel, D. 1990. Effects of prostaglandin E_2 on production of new cancellous bone in the axial skeleton of ovariectomized rats. Bone 11:103-113.
15) Jee, W.S.S., Mori, S., Li, X.J., and Chan, S. Prostaglandin E_2 enhances cortical bone mass and activates intracortical bone remodeling in intact and ovariectomized female rats. Bone (in press).
16) Li, X.J., Jee, W.S.S., Li, Y.L., and Patterson-Buckendahl, P. Transient effects of subcutaneously administered prostaglandin E_2 on cancellous and cortical bone in young adult dogs. Bone (in press).
17) Polig, E., and Jee, W.S.S. Hit rates and radiation doses in nuclei of bone-lining cells from alpha-emitting radionuclides. Radiat. Res. (Submitted).
18) Mori, S., Li, X.J., and Jee, W.S.S. Production of new trabecular bone in osteopenic ovariectomized rats by prostaglandin E_2. Calcif. Tissue Int.(submitted).

19) Li, X.J., and Jee, W.S.S. Adaptation of diaphyseal structure with aging and decreased mechanical loading in the adult rat: a densitometric and histomorphometric study. Anat. Rec. (submitted).
20) Jee, W.S.S., Li, X.J., and Schaffler, M.B. Adaptation of diaphyseal structure with aging and increased mechanical loading in the adult rat: A densitometric histomorphometric and biomechanical study. Anat. Rec. (submitted).
21) Woodard, J.C., and Jee, W.S.S. Skeletal System. In: Fundamentals of Toxicologic Pathology. (W.M. Haschecк-Holik and C. Rousseaux, eds.), Academic Press (in press).
22) Jee, W.S.S. Introduction to Skeletal Function. In: A Basic Science Primer in Orthopaedics. (R.F. Worell and F. Bronner, eds.), William & Wilkins (in press).
23) Miller, S.C., and Jee, W.S.S. Bone-lining Cells. In: Bone: A Treatise. (B.K. Hall, ed.) (in press).
24) Bruenger, F., Polig, E. and Jee, W.S.S. Local distribution of ^{239}Pu using digitized images of neutron-induced autoradiographs. Radiation Protection Dosimetry (submitted).

A. Accomplishments.

1) Task I. Cells at Risk

1. Bone cell kinetics of endocortical remodeling in the rat.

In this study, groups of rats were killed after 3, 7 and 14 day of lactation on a low calcium diet and 1, 3, 5, 7 and 14 days post lactation on a normocalcemic diet (recovery) to study the sequence of long bone remodeling. All animals were give ^{3}H-thymidine (one hour before sacrifice) and ^{3}H-proline (four and one day before sacrifice) and double-labeled with fluorescent bone markers (eight and one day before sacrifice). Table I.1, Figures I.1 and I.2 summarize the qualitative information on the bone remodeling responses (i.e., activation, resorption and formation) at the cortical surfaces (i.e., periosteal and endocortical).

TABLE I.1. Sequential Cellular Changes on Various Cortical Bone Surface

Experimental periods (Day)	Endocortical Surface			Periosteal Surface		
	Resorption	Formation		Resorption	Formation	
		Osteoid	Labeled		Osteoid	Labeled
0	rare	rare	rare	0	rare	rare
L3(loCa)	40%	0	0	0	0	0
L7(loCa)	100%	0	0	0	0	0
L14(loCa)	80%	20%	4%	0	0	0
L21(loCa)	0	100%	30%	0	rare	0
R1(nor Ca)	0	100%	80%	0	rare	0
R3(nor Ca)	0	100%	80%	0	rare	0
R5(nor Ca)	0	90%	85%	0	rare	0
R7(nor Ca)	0	70%	85%	0	rare	0
R13(nor Ca)	0	50%	40%	0	rare	0

Day 0 is the final day of pregnancy; Ln is day n of lactation period; Rn is day n of recovery period.
lo Ca is low calcium diet; nor Ca is normal calcium diet.

Skeletal responses were limited to endocortical surface, periosteal surface was inactive. During lactation plus low calcium period, massive resorption was observed at day 3 and it occupied the entire endocortical surface at day 7. However, endocortical resorption began to decrease at day 14 and completely suppressed at day 21. Unexpectedly, despite the continues severe calcium deficiency, 20% of the endosteal surface was forming bone at day 14 and it extended to all previously resorbed surfaces which including both endocortical and all intracortical cavity surfaces at day 21. We had previously assumed that the reversal phase (bone formation) would not begin until rats were placed on a normo-calcium diet. Furthermore, the bone matrix formed during lactation plus low calcium period was uncalcified and did not mineralize until the rats were allowed free access to a normal calcium diet.

Table I.2, Figures I.1 and I.2 summarize the structural and histologic morphometry and ^{3}H-thymidine cell labeling changes. The loss of percent cortical bone area began at day 7 and progressively increased to about 25% of day 0 value at day 21 of lactation plus low calcium. This resulted from an increase of both percent marrow area (+40%) and percent porosity area (from 0 to 5.6%). At day 14 of recovery period on a normal calcium diet, 23% of the lost cortical bone was restored by the closure of intracortical resorption cavities and the reduction of the marrow area. At day 7 of lactation plus low calcium diet, there was a 11-fold increase in percent osteoclastic surface (45% osteoclastic surface), and at day 21 of lactation plus low calcium diet, there was a 9-fold increase in percent osteoclastic surface (66% osteoblastic surface). ^{3}H-proline labeled bone appeared at day 14 of lactation plus low calcium.

^{3}H-thymidine is incorporated into all proliferating cells during DNA synthesis. Labeled cells adjacent to osteoclasts or osteoblasts are believed to be their precursor cells (pre-osteoclasts or pre-osteoblasts). The labeled "pre-osteoclasts" were numerous while the labeled "pre-osteoblasts" were rare (Figs. I.3). Our current analysis did not separate these two functional sites. ^{3}H-thymidine labeled cells near bone surfaces rose abruptly at day 3 of lactation and peaked at 3.3 times of day 0 values at day 7 of lactation. Surprisingly at day 3 of recovery onward, labeled cells returned to pre-lactation values. ^{3}H-thymidine labeled cells in the marrow proper rose 1.2 times on day 7 of lactation, remain high level until day 21 of lactation, returned to normal level at day 3 of recovery and decreased from that thereafter (Table I.2).

Table I.2 SEQUENTIAL CHANGES OF CORTICAL BONE HISTOMORPHOMETRY AND 3H-THYMIDINE LABELED CELLS

Experimental Period (day)		Tissue Area (mm^2)	Percent Cortical Area (%)	Percent Marrow Area (%)	Percent Porosity Area (%)	Endosteal Osteoclastic surface (%)	Endosteal Osteoblastic surface (%)	3H-Thymidine Labeled Cells (near bone surface) (#/field)	3H-Thymidine Labeled Cells (Marrow center) (#/field)
Lactation + Low calcium diet									
L0	Mean	5.26	70.19	29.81	0.000	3.8	6.8	8.5	7.2
	SD	0.21	4.26	4.26	0.000	0.7	1.2	2.8	1.7
L3	Mean	4.89	72.63	27.37	0.000	24.6	10.0	23.5	7.7
	SD	0.32	0.40	0.40	0.000	3.5	0.6	4.8	3.5
	%	**93**	**103**	**92**	**0**	**650#**	**148***	**275***	**106**
L7	Mean	5.26	62.80	36.31	0.884	44.8	11.6	27.8	16.0
	SD	0.06	2.50	2.80	0.432	5.4	3.0	8.9	4.2
	%	**100**	**89**	**122**	*	**1184@**	**171***	**326***	**221***
L14	Mean	4.95	53.20	42.17	4.627	41.4	37.9	18.9	11.0
	SD	0.16	3.43	3.35	0.083	4.7	1.6	2.3	5.3
	%	**94**	**76#**	**141***	**@**	**1095@**	**561@**	**221#**	**153**
L21	Mean	4.89	52.90	41.49	5.614	24.1	66.2	18.6	14.6
	SD	0.20	3.11	3.15	0.040	1.8	12.6	3.5	5.3
	%	**93**	**75***	**139***	**@**	**638@**	**980@**	**218***	**201**
Recovery + Normal calcium diet									
R1	Mean	5.31	52.14	42.83	5.033	5.4	81.0	16.7	10.8
	SD	0.12	3.51	3.35	0.412	4.7	2.9	4.2	3.3
R3	Mean	5.12	60.22	37.28	2.505	0.0	100.0	8.2	5.3
	SD	0.14	3.81	4.60	0.805	0.0	0.0	1.7	0.5
	%-1	**96**	**115**	**87**	**50#**		**123@**	**49***	**49***
R5	Mean	5.05	61.39	37.72	0.888	0.0	79.4	9.1	5.6
	SD	0.28	1.36	1.46	0.106	0.0	2.6	1.5	1.6
	%-1	**95**	**118***	**88**	**18@**		**98**	**55***	**52**
R7	Mean	4.87	61.30	37.96	0.736	0.0	33.3	9.2	4.4
	SD	0.35	4.36	4.43	0.067	0.0	17.7	1.2	0.8
	%-1	**92**	**118**	**89**	**15@**		**41***	**55***	**41**
R14	Mean	5.33	64.18	35.64	0.182	0.0	19.7	6.2	3.7
	SD	0.13	1.69	1.43	0.258	0.0	1.4	0.8	0.7
	%-1	**100**	**123***	**83**	**4@**		**24@**	**37***	**34**

%: percent of L0; %-1: percent of R1; *p < 0.05; #p < 0.01; @p < 0.001.

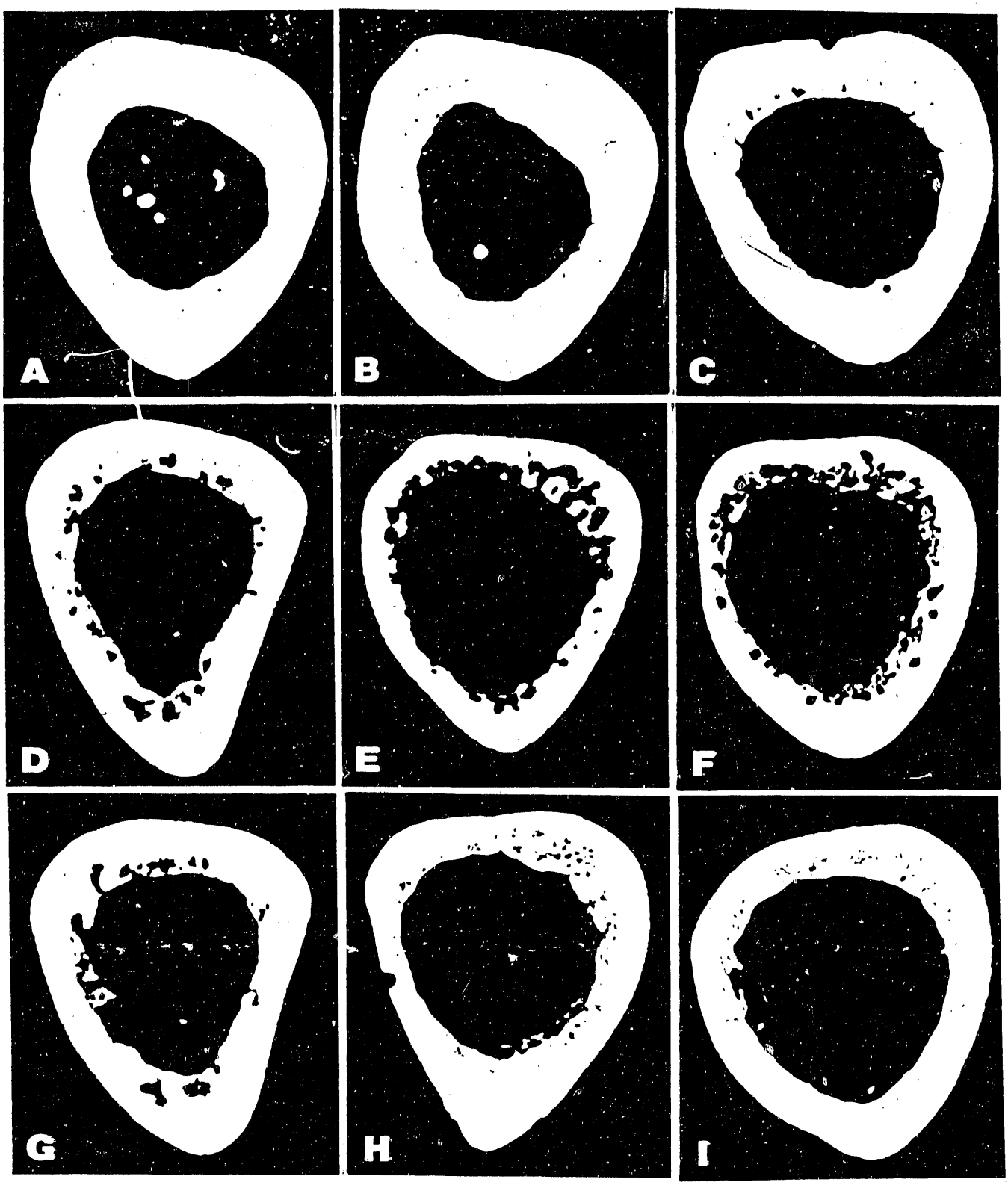

Fig. 1.1 Stages in the pregnancy, lactation with low calcium diet and recovery on normocalcium diet (rat cortical bone remodeling system). Microradiograph of tibial shafts. A. L0 stage. First day on lactation and low Ca. B. L3 stage. Day 3 on lactation and low Ca. Enlarged marrow cavity. C. L7 stage. Day 7 on lactation and low Ca. Enlarged marrow and beginning intracortical porosity. D. L14 stage. Day 14 of lactation and low Ca. Enlarged marrow and increased intracortical porosity. E. L21 stage. Day 21 on lactation and low Ca. Massive endosteal resorption resulting in enlarged marrow cavity and thinned cortex. F. Day 3 on recovery on normal Ca. The early filling of resorption space. G. R5 stage. Day 5 of recovery and normal Ca. Partial filling of resorption spaces. H. R7 stage. Day 7 of recovery. Nearly complete intracortical resorption cavity filling. I. Day 14 of recovery and normal Ca. Incomplete recovery with enlarged marrow cavity but completed filling of intracortical porosity. X30.

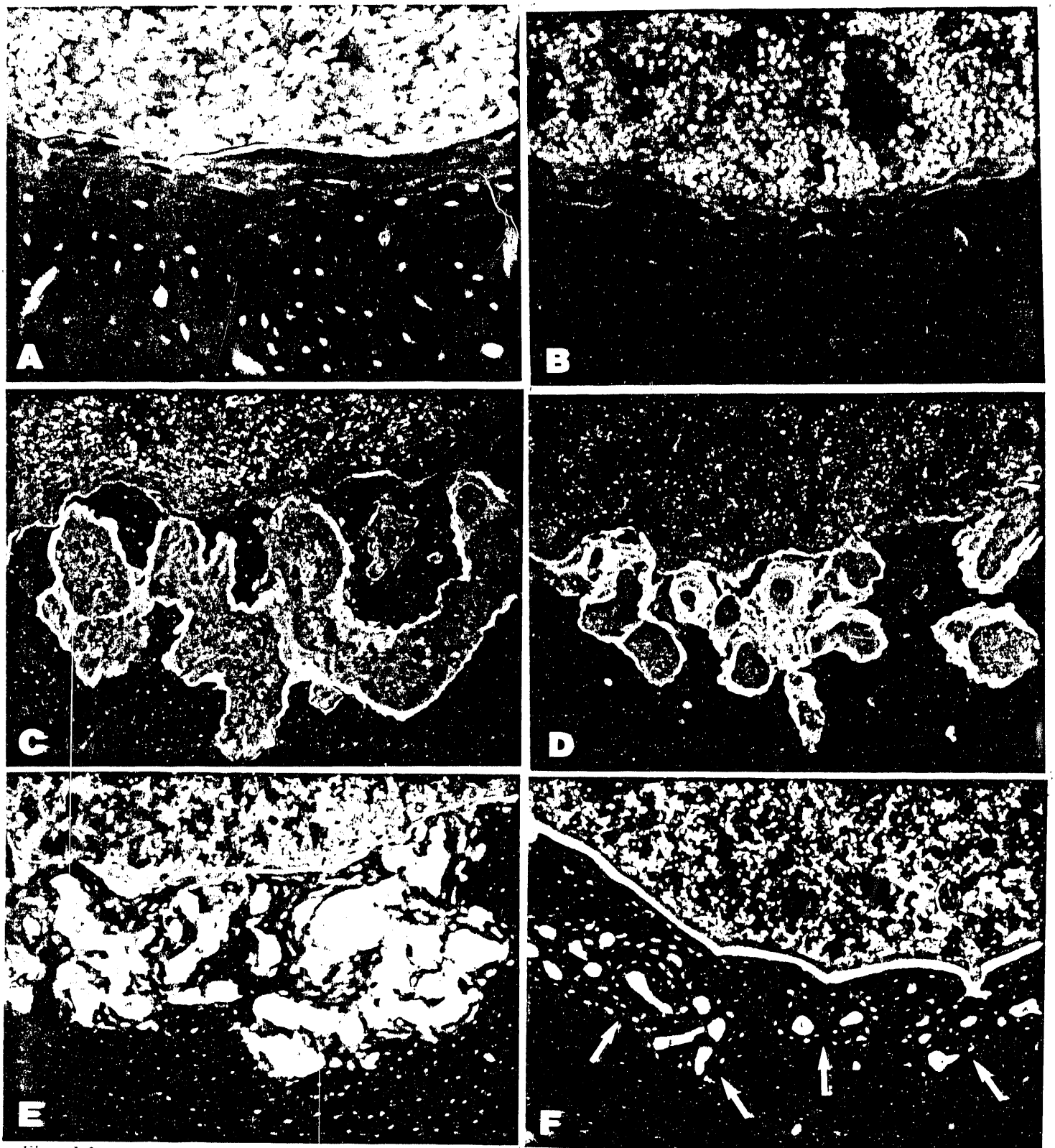

Fig. I.2. The appearance of the endocortical surface during days 0, 7, and 21 of lactation and low calcium diet (L0, 7, and 21) and days 3, 7, and 14 of recovery on normal calcium diet (R3, 7, and 14). A. L0 stage. Several bone forming sites lined with osteoid (orange) and fluorescent label (green). B. L7 stage. Entire surface covered by osteoclasts in shallow Howship's lacunae. C. L21 stage. Huge Howship's lacunae mostly covered with osteoid (orange) and some newly mineralized bone (green). D. R3 stage. Progressive filling of lacunae with osteoid (orange) and mineralized matrix (green). E. R7 stage. Continued filling of lacunae with mineralized bone (green) and osteoid. F. R14 stage. Filling of Howship's lacunae with osteon-like structures (arrows). Fluorescent micrograph of 20 micron undecalcified section X150.

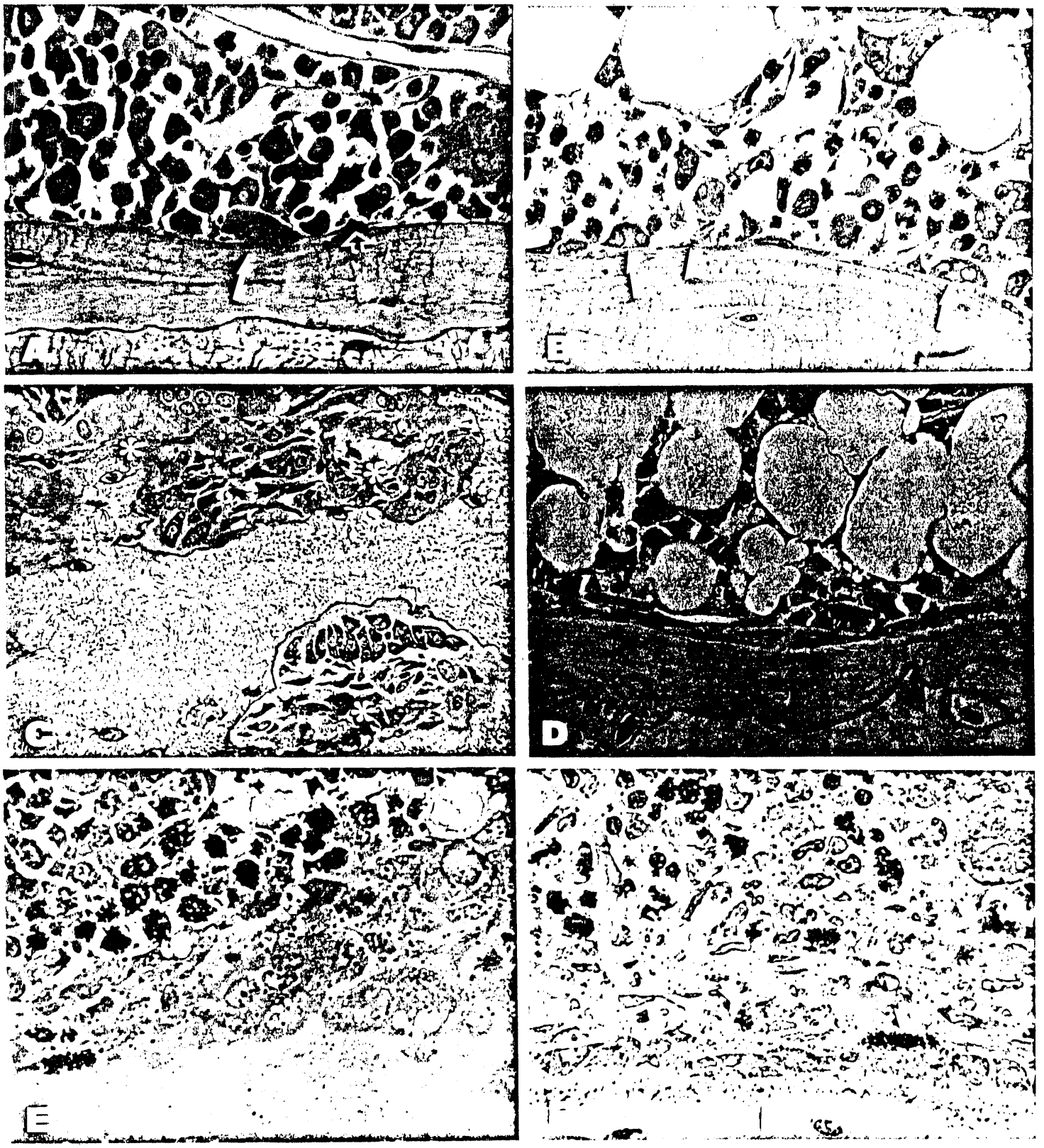

Fig I.3. Sequential changes of endocortical cellular distribution during days 0, 3, and 14 of lactation plus low calcium diet (L0, 3, 14) and during days 3 and 7 of recovery on normal calcium diet (R3 and 7) stages. A. L0 stage. A single osteoclast (arrow) and retracted bone lining cell (open arrow) residing on smooth bone surface. B. L3 stage. Two osteoclasts (arrows) and bone lining cells (arrow head) on a smooth bone surface. C. L14 stage. Massive influx of osteoclasts (*) with appearance of osteoblasts nearby. D. R7 stage. Bone-lining cells covering just completed bone forming surface. E. L7 stage. Cluster ^{3}H-thymidine labeled cells adjacent to colony of large multinucleated osteoclasts. F. R3 stage. Labeled preosteoblasts (arrows) adjacent to osteoblast layer. Note. ^{3}H-proline labeling of bone matrix proper (arrow head). Micrograph of 1 micron decalcified section X800.

Most rewarding was the appearance of numerous bone-lining cells at day 7 of recovery (Fig. I.3). In future studies with proper control and the employment of series sacrifice after multiple ^{3}H-thymidine labeling methodology, we will be able to determine the origin of bone lining cells if they are ^{3}H-thymidine labeled. Thereafter, we will also be able to trace their fate.

2. Bone lining cells: structure and function (a review)

Bone lining cells (BLC's) cover inactive (resting) bone surfaces, particularly evident in the adult skeleton. BLC's are thinly extended over bone surfaces, have flat or slightly ovoid nuclei, connect to other BLC's via gap junctions, and send cell processes into surface canaliculi. BLC's can be induced to proliferate and differentiate into osteogenic cells and may represent a source of "determined" osteogenic precursors in birds. Direct evidence from mammals suggest that BLC's are capable of giving rise to osteoblasts when it is needed. BLC's and other cells of the endosteal tissues may be an integral part of the marrow stromal system and have important functions in hematopoiesis, perhaps by controlling the inductive microenvironment. Because activation of bone remodeling occurs on inactive bone surfaces, BLC's may be involved in the propagation of the activation signal that initiates bone resorption and bone remodeling. (Miller, S.C., de Saint Georges, L., Bowman, B.M. and Jee, W.S.S. Bone lining cells: Structure and function. Scanning microscopy. 3: 953-961, 1989).

Importance: This exciting model will enable us to characterize the bone cells involved in bone remodeling within the range of alpha-emitting bone-seeking radionuclides.

2) Task II. Bone Cell Residence Time

The specific aim of this part of the program is to improve our knowledge of bone cell residence time. The residence-time is mainly influenced by bone turnover rates. The deposition and redistribution of bone-seeking radionuclides are heavily influenced by bone architecture and by the process of bone turnover, information badly needed in our bone cell-specific dosimetry program.

We have enlarged our information on bone turnover rates by characterizing the static and dynamic histomorphometry of select cortical and cancellous bone sites in three and nine year old beagle dog skeletons. We have studied the impact of body weight by comparing properties of select cortical and cancellous bone in St. Bernard (a 50 kg dog) and Beagle (a 10-12 kg dog) skeletons, and the influence of mechanical usage (underloading and overloading) in an unilaterally rear-immobilized adult rat model, information needed to extrapolate to people. These studies are summarized as follows.

I. Static and Dynamic Histomorphometry of Select Cortical and Cancellous Bone Sites.

Three and nine year old Beagles were studied. The cortical bone sites included the mid-femoral, proximal humeral, distal humeral, mid-humeral, mid-tibial, mid-metatarsal and rib shafts.

The cancellous bone sites involved the proximal tibial, proximal humeral and distal femoral metaphyses, caudal and lumbar vertebral bodies, iliac creast and proximal metatarsal epiphysis.

(1) The major differences between cortical and cancellous bone are its percent mass, surface to volume ratio, and bone turnover rates. (Table II.1).

(2) In seven cancellous bone sampling sites, we found that most cancellous bone sites are similar in histomorphometry. The exception is that in the epiphyseal cancellous bone sites there are more bone, smaller surface to volume ratio and lower turnover rates (greater than one order of magnitude). (Tables II. 2, 3).

(3) In six cortical bone sampling sites, we found cortical bone morphometry can be quite variable. One extreme is the mid-femoral shaft with plenty of inner and outer circumferential lamellae that is being remodeled. The other extreme is the rib with greater than average surface to volume ratio, more inner circumferential lamellae and high turnover rate (at least a factor of six greater than other cortical bone sites). (Tables II. 4-7).

TABLE II.1. DIFFERENCES BETWEEN CORTICAL AND CANCELLOUS BONES (BEAGLE)

Parameters	Units	Cortical	Cancellous
Mass	%	98	22
Surface/Volume	cm/cm^2	55	180
Mineral Appositional Rate	µm/d	0.77	0.66
Bone Formation Rate	%/y	43	1.46

TABLE II.2. VARIATION IN CANCELLOUS BONE CHARACTERISTICS (BEAGLES)*

Site	More	Less
Metatarsal head	Percent mass	Surface/volume
(epiphysis)	Formation period	Label surface
		Bone formation rate
Caudal vertebra	Per cent mass	Labeled surface
		Bone formation surface
Iliac crest	Bone formation rate	

*Sites include proximal tibial metaphysis, metatarsal head, caudal vertebral body, proximal humeral metaphysis, distal femoral metaphysis, iliac crest and lumbar vertebral body.

II. Comparison of St. Bernard and Beagle Bone: The Impact of Body Weight.

It has been postulated that larger body size dogs have increased bone metabolism due to higher mechanical loading. St. Bernards have 5 times as much body weight as Beagles and it has been also postulated that because of the mechanical loading on the skeleton from the larger body size, St. Bernards develop primary osteosarcomas 60 times more than Beagles. The aim of this study was to assess bone mass and bone formation in cancellous and cortical bone sites of the larger St. Bernard and the smaller Beagle dogs.

Four St. Bernards and 4 Beagles (mean age: 6 years old) were double labeled and seven cancellous and six cortical bone sites were examined by histomorphometry. The St. Bernards were observed to be physically much less active than the Beagles.

Compared to Beagle skeleton, St. Bernards' cancellous sites have lower percent trabecular bone, trabecular number, and higher mineral apposition and bone formation rates. St. Bernards' cortical sites have greater total tissue, percent marrow volume, percent porosity, higher mineral apposition rate but less percent bone. Also these less active St. Bernards have higher bone remodeling rates than the Beagle. The lesser available bone surface and the higher bone formation may contribute to the higher incidence of osteosarcoma in the larger breed (Tables II.3, 5, 8 and 9). (Mori, S., Li, X.J. and Jee, W.S.S. Skeletal histomorphometry in large and small dogs: Influence of body size [in preparation]).

Table II.3 CANCELLOUS BONE HISTOMORPHOMETRY OF ST. BERNARD AND BEAGLE DOG BONES

St. Bernard	Tb.Ar	Tb.Th	Tb.N	Tb.Sp	S/V	W.Wi	LS	MAR	MLT	BFR	FP
Analysis of Variance	0.0001	0.0001	0.0079	0.0080	0.0001	0.0075	0.0366	0.0001	0.0067	0.0010	0.0001
Proximal Tibia	13.26	87.00	1.53	844.48	19.38	54.19	9.56	1.08	9.88	73.69	50.45
SD	2.78	10.52	0.29	210.63	2.32	2.81	2.79	0.08	1.21	26.85	3.83
Metatarsal Head	24.33	140.63	1.74	638.68	11.87	43.93	2.25	0.79	11.05	8.14	58.11
SD	2.71	4.98	0.25	114.73	0.41	3.12	1.35	0.18	2.07	5.67	14.72
Cadual Vertebra	25.54	123.95	2.07	524.41	13.74	56.18	9.79	0.90	10.97	43.37	62.84
SD	4.36	20.43	0.27	86.55	2.29	4.72	4.11	0.07	0.81	17.22	6.83
Proximal Humerus	20.47	116.92	1.76	650.82	14.53	46.27	10.74	1.03	13.08	65.84	46.49
SD	2.67	19.07	0.07	19.55	2.20	0.70	4.49	0.21	3.85	44.56	11.14
Distal Femur	13.46	93.27	1.43	874.12	18.30	50.52	9.03	1.06	10.22	66.66	48.11
SD	3.19	16.58	0.11	100.42	3.14	1.78	2.49	0.11	1.42	30.78	5.77
Iliac Crest	14.35	81.42	1.77	704.46	20.83	50.98	9.62	1.38	8.94	100.90	37.51
SD	2.16	12.23	0.25	101.95	3.07	3.04	2.07	0.16	4.15	28.60	6.02
Lumbar Vertebra	19.31	127.29	1.54	772.00	13.32	51.79	11.95	1.22	9.61	70.09	42.84
SD	2.18	18.62	0.25	151.26	1.97	3.38	1.74	0.15	4.67	9.52	6.95
Mean	18.67	110.07	1.69	715.61	16.00	50.55	8.99	1.07	10.54	61.24	49.48
SD	5.49	25.45	0.28	160.33	3.86	4.82	3.92	0.22	2.92	35.83	11.17

Beagle	Tb.Ar	Tb.Th	Tb.N	Tb.Sp	S/V	W.Wi	LS	MAR	MLT	BFR	FP
Analysis of Variance	0.0001	0.0001	0.0137	0.0085	0.0001	0.0002	0.0042	0.0003	0.5712	0.0033	0.0074
Proximal Tibia	19.12	83.03	2.31	505.06	20.55	45.95	8.16	0.53	15.15	30.69	95.90
SD	3.18	15.33	0.19	49.42	3.36	2.29	3.19	0.08	5.15	17.05	15.02
%	44*	-5	51#	-40*	6	-15#	-15	-51@	53	-58*	90#
Metatarsal Head	29.39	132.41	2.24	456.49	12.81	36.88	1.83	0.46	17.92	3.39	89.75
SD	2.67	19.07	0.23	47.12	1.97	2.29	0.55	0.08	2.79	0.34	13.83
%	21*	-6	29*	-29*	8	-16*	-19	-42*	62#	-58	54*
Cadual Vertebra	26.00	97.88	2.66	400.92	17.14	43.90	5.19	0.81	10.76	24.29	59.59
SD	2.35	8.50	0.08	20.64	1.49	3.55	2.13	0.05	0.85	10.44	6.72
%	2	-21	28#	-24*	25*	-22#	-47	-10	-2	-44	-5
Proximal Humerus	19.67	89.77	2.19	530.21	18.59	42.90	10.39	0.97	14.92	63.82	48.69
SD	1.36	2.62	0.20	57.64	0.56	2.97	2.21	0.13	1.97	21.64	4.03
%	-4	-23*	25#	-19#	28*	-7	-3	-6	14	-3	5
Distal Femur	19.12	76.77	2.52	470.60	21.98	41.88	9.71	0.73	16.18	52.18	63.46
SD	2.07	9.39	0.38	73.52	2.76	1.41	3.85	0.07	3.85	22.31	7.35
%	42*	-18	76#	-46@	20	-17@	8	-32#	58*	-22	32*
Iliac Crest	19.89	79.09	2.53	457.82	21.25	44.48	11.51	1.03	11.53	85.16	48.01
SD	0.76	8.18	0.22	40.02	2.05	4.46	2.93	0.18	1.96	31.25	5.99
%	39#	-3	43#	-35#	2	-13	20	-26*	29	-16	28*
Lumbar Vertebra	22.03	107.96	2.03	554.19	15.79	44.75	10.60	0.85	10.38	44.44	58.42
SD	4.90	19.07	0.09	57.06	2.57	2.80	8.88	0.11	0.93	33.20	11.66
%	14	-15	32#	-28*	19	-14*	-11	-30#	8	-37	36
Mean	22.17	95.27	2.35	482.14	18.30	42.96	8.20	0.77	13.83	43.43	66.26
SD	4.51	21.87	0.28	66.74	3.70	3.84	4.94	0.22	3.76	32.09	20.05
%	19	-13	39*	-33*	14	-15*	-9	-28	31	-29	34

TABLE II.4. VARIATION IN CORTICAL BONE CHARACTERISTICS (BEAGLES)

Site	More	Less
Proximal humeral shaft	Cross section area Marrow area Resorption period	Primary bone Primary bone porosity Outer[1] and inner[2] primary bone
Femoral Shaft	Primary bone area Primary bone porosity Outer primary bone	Osteonal bone
Tibial shaft Humeral shaft	Primary bone porosity	Primary bone area Inner primary bone
Metatarsal shaft	Surface/volume porosity Osteonal porosity Formation period Activation frequency	Cross section area porosity Cortical area Marrow area Primary bone porosity Label surface
Rib	Surface/volume porosity Osteonal porosity Inner primary bone Bone formation rate Activation frequency	Cross section Cortical Mineral appositional rate Primary bone porosity

[1]Outer primary bone - circumferential lamellae and primary osteons.
[2]Inner primary bone - circumferential lamellae

Table II.5 CORTICAL BONE HISTOMORPHOMETRY OF ST. BERNARD AND BEAGLE DOG BONES

St. Bernai	T.Ar	Ct.Ar	%Ct.Ar	M.Ar	%M.Ar	%Por	CtB.Ar	%CtB.Ar	LS	MAR	BFR	MLT	FP	RP	Acf
ANOVA	0.0001	0.0001	0.0001	0.0001	0.0001	0.0001	0.0001	0.0001	0.342	0.7032	0.0005	0.0002	0.0149	0.2123	0.0003
DH	412.26	156.72	38.63	255.55	61.38	2.60	152.69	37.59	0.052	1.13	2.12	8.66	51.48	19.86	0.80
SD	67.54	8.75	5.02	59.11	5.02	1.04	9.60	4.53	0.017	0.13	0.62	1.02	5.29	6.37	0.31
FS	367.08	133.66	36.48	233.42	63.53	0.74	132.63	36.21	0.051	1.10	2.02	9.29	54.11	9.68	1.73
SD	54.24	18.30	1.80	37.78	1.80	0.64	17.67	1.95	0.019	0.09	0.66	1.47	4.59	5.57	0.25
HS	361.75	138.35	38.99	223.41	61.01	0.94	137.04	38.63	0.057	1.10	2.23	9.31	54.06	14.46	1.71
SD	74.02	14.83	4.99	60.25	4.99	0.24	14.53	4.95	0.025	0.07	0.86	1.01	2.40	2.06	0.25
PH	607.00	138.79	22.82	468.21	77.18	11.88	122.45	20.15	0.098	1.05	3.80	10.66	55.86	19.46	1.26
SD	59.29	30.13	3.79	46.61	3.79	2.81	27.68	3.71	0.035	0.11	1.54	1.05	6.64	3.08	0.43
Rib	58.54	21.48	37.00	37.06	63.00	3.66	20.70	35.69	0.264	1.15	11.24	10.02	46.95	17.63	5.37
SD	5.41	1.65	5.09	6.24	5.09	1.34	1.65	5.26	0.128	0.11	5.99	1.43	6.61	5.20	1.88
TS	68.46	40.05	58.32	28.41	41.68	2.80	39.03	56.71	0.073	1.03	2.69	5.37	75.61	18.19	3.54
SD	19.63	13.18	5.77	8.36	5.77	1.66	13.22	6.01	0.030	0.20	0.71	1.24	21.71	10.64	2.09
Mean	312.51	104.84	38.71	207.67	61.29	3.77	100.75	37.50	0.099	1.09	4.02	8.88	56.34	16.55	2.40
SD	203.80	56.31	11.35	156.29	11.35	4.08	54.20	11.58	0.092	0.12	4.06	2.04	12.88	6.52	1.92

Beagle	T.Ar	Ct.Ar	%Ct.Ar	M.Ar	%M.Ar	%Por	CtB.Ar	%CtB.Ar	LS	MAR	BFR	MLT	FP	RP	Acf
ANOVA	0.0001	0.0001	0.0004	0.0001	0.0004	0.1523	0.0001	0.0006	0.269	0.0001	0.0003	0.0001	0.0001	0.0021	0.0001
DH	83.71	61.56	73.84	22.15	26.16	0.97	60.97	73.13	0.02	0.73	0.62	10.55	67.69	62.83	0.40
SD	8.27	2.88	4.31	5.76	4.31	0.49	2.98	4.33	0.01	0.21	0.54	2.09	21.24	28.90	0.34
	-80@	-61@	91@	-91@	-57@	-63*	-60@	95@	-60*	-35*	-71*	22	31	216*	-50
FS	88.01	55.62	64.43	32.39	35.57	0.25	55.49	64.28	0.03	0.53	0.55	14.62	84.48	18.07	1.13
SD	21.13	8.04	8.90	15.04	8.90	0.14	8.06	8.93	0.01	0.04	0.14	1.96	9.84	5.74	0.20
	-76@	-58@	77@	-86@	-44@	-67	-58@	78@	-44	-52@	-73#	57#	56#	87	-35#
HS	79.54	58.86	74.30	20.68	25.70	0.77	58.38	73.74	0.03	0.53	0.56	16.55	96.51	27.40	1.01
SD	11.43	6.41	3.51	5.51	3.51	0.44	6.10	3.74	0.01	0.06	0.11	1.88	12.24	8.61	0.22
	-78@	-57@	91@	-91@	-58@	-17	-57@	91@	-47	-52@	-75#	78@	79@	89*	-41#
PH	139.27	65.57	47.51	73.70	52.49	2.40	64.00	46.42	0.04	0.92	1.28	9.19	54.58	23.45	1.01
SD	22.71	6.86	4.26	17.40	4.26	2.11	6.88	4.87	0.01	0.08	0.61	1.89	10.04	5.32	0.14
	-77@	-53#	108@	-84@	-32@	-80#	-48#	130@	-62*	-13	-66*	-14	-2	21	-20
Rib	15.45	8.29	56.07	7.16	43.93	2.59	8.08	54.72	0.16	0.85	5.10	7.84	60.22	19.03	4.90
SD	4.83	1.06	10.64	4.01	10.64	1.96	1.06	11.07	0.06	0.20	2.86	1.24	17.91	7.98	1.41
	-74@	-61@	52*	-81@	-30*	-29	-61@	53*	-41	-26*	-55	-22	28	8	-9
TS	21.74	17.54	79.89	4.20	20.12	2.08	17.20	78.41	0.04	0.41	0.63	14.22	164.04	39.23	1.63
SD	7.83	8.03	14.52	2.90	14.52	1.85	7.92	15.36	0.03	0.06	0.42	3.21	20.32	12.22	1.13
	-68#	-56*	37*	-85#	-52*	-26	-56*	38*	-44	-60#	-77#	165#	117#	116*	-54
Mean	71.29	44.57	66.01	26.71	33.99	1.51	44.02	65.12	0.052	0.66	1.46	12.16	87.92	31.67	1.68
SD	44.98	23.86	13.87	25.19	13.87	1.55	23.60	14.11	0.054	0.22	2.00	3.73	40.26	20.20	1.66
	-77	-57	71*	-87	-45*	-60	-56	74*	-47	-40*	-64	37	56	91	-30

Table II.6 **MORPHOLOGICAL PARAMETERS OF VARIOUS CORTICAL SITES OF BEAGLE DOG**

Bone Site	Primary Cortical Region				Secondary Cortical Region				Primary to Secondary Cortical Area (ratio)	Primary to Secondary Porosity Density (ratio)	% Outer Primary Area of Cortical Area (%)	% Inner Primary Area of Cortical Area (%)
	Bone Area (%)	Percent Porosity Area (%)	Porosity Density (#/mm^2)	Size of Porosity (μm^2)	Bone Area (%)	Percent Porosity Area (%)	Porosity Density (#/mm^2)	Size of Porosity (μm^2)				
Analysis of Variance	0.0002	0.0003	0.0039	0.0740	0.0002	0.2262	0.0001	0.6988	0.0011	0.0214	0.0001	0.0322
Mid-Femoral Shaft	55.66	0.76	12.49	0.71	44.34	5.35	67.40	0.84	1.29	0.18	42.91	12.75
SD	6.37	0.26	4.43	0.48	6.37	5.02	7.85	0.82	0.36	0.05	9.19	6.60
Rank	1	3	3	4	7	3	1	6	1	5	1	2*
Proximal Humeral Shaft	15.32	0.18	3.80	0.45	84.68	3.66	28.49	1.35	0.18	0.13	7.49	7.83
SD	4.64	0.12	2.54	0.24	4.64	0.69	7.84	0.42	0.06	0.07	1.99	3.22
Rank	7	6	7	5	1	5	7	1	7	6	7	5
Distal Humeral Shaft	31.30	0.55	7.62	0.72	68.70	3.95	41.02	0.96	0.48	0.20	19.57	11.73
SD	9.10	0.24	2.49	0.17	9.10	1.55	9.70	0.25	0.21	0.09	8.40	3.00
Rank	4	4	5	3	4	4	5	4	4	4	4	3
Mid-Humeral Shaft	29.86	1.11	13.42	1.10	70.14	3.04	42.54	0.72	0.45	0.34	23.08	6.78
SD	9.28	0.63	7.27	0.99	9.28	1.95	9.64	0.39	0.21	0.20	10.60	2.55
Rank	5	1	2	1	3	7	4	7	5	2	3	7
Mid-Tibial Shaft	20.78	0.85	12.05	0.87	79.22	3.21	35.22	0.94	0.27	0.36	13.61	7.17
SD	6.27	0.26	4.57	0.58	6.27	1.16	6.81	0.36	0.10	0.17	5.69	4.95
Rank	6	2	4	2	2	6	6	5	6	1	6	6
Mid-Metatarsal Shaft	37.07	0.19	19.30	0.11	62.93	7.79	65.86	1.28	0.60	0.30	25.96	11.11
SD	5.53	0.03	8.56	0.04	5.53	5.76	12.28	1.01	0.13	0.14	5.57	2.33
Rank	2	5	1	7	6	2	2	2	3	3	2	4
Rib	36.41	0.08	4.83	0.16	63.59	7.79	64.93	1.19	0.70	0.07	18.10	18.31
SD	17.43	0.04	0.62	0.08	17.43	3.64	9.41	0.48	0.63	0.01	10.30	7.78
Rank	3	7	6	6	5	1	3	3	2	7	5	1
Mean	**32.34**	**0.53**	**10.50**	**0.59**	**67.66**	**4.97**	**49.35**	**1.04**	**0.57**	**0.23**	**21.53**	**10.81**
SD	**14.74**	**0.45**	**6.80**	**0.55**	**14.74**	**3.56**	**17.38**	**0.57**	**0.44**	**0.15**	**12.68**	**5.70**

Table II.7

MORPHOLOGICAL PARAMETERS OF VARIOUS CORTICAL SITES OF BEAGLE DOG

Bone Site	Total Cross Sectional Area (mm^2)	Cortical Area (mm^2)	Cortical Bone Area (mm^2)	Marrow Area (mm^2)	Percent Porosity Area (%)	Porosity Density (#/mm^2)	Size of Porosity (μm^2)	Surface to Volume (mm/mm^2)	% Porosity Perimeter of total Perimeter (%)	% Periosteal Perimeter of total Perimeter (%)	% Endosteal Perimeter of total Perimeter (%)	Periosteal to Endosteal Perimeter (ratio)
Analysis of Variance	0.0001	0.0001	0.0001	0.0001	0.2090	0.0014	0.8223	0.0006	0.0001	0.0001	0.0001	0.1177
Mid-Femoral Shaft	80.67	47.74	46.21	32.93	3.07	36.96	0.95	4.80	74.85	15.42	9.74	1.60
SD	21.15	6.15	5.31	16.17	1.97	7.98	0.82	0.74	0.88	1.39	0.75	0.26
Rank	3	5	5	2	4	3	6	5	4	4	4	5
Proximal Humeral Shaft	143.94	61.36	58.64	82.58	3.15	24.68	1.34	4.90	60.99	22.15	16.86	1.32
SD	39.26	9.60	8.02	31.34	0.54	6.42	0.41	0.34	2.84	1.16	1.84	0.18
Rank	1	1	1	1	3	7	1	3	7	1	1	7
Distal Humeral Shaft	81.15	58.34	56.67	22.81	2.88	30.10	0.97	4.52	77.60	13.80	8.60	1.60
SD	9.36	3.80	3.95	5.82	0.64	4.90	0.23	0.69	2.29	1.79	0.68	0.17
Rank	2	2	2	3	6	6	4	7	2	6	5	4
Mid-Humeral Shaft	74.59	54.10	52.72	20.48	2.57	33.61	0.80	4.86	78.94	13.40	7.66	1.78
SD	13.02	6.49	6.40	6.76	1.07	7.03	0.37	1.37	4.84	2.82	2.23	0.23
Rank	5	4	4	5	7	4	7	4	1	7	7	3
Mid-Tibial Shaft	77.42	54.84	53.22	22.59	2.90	30.63	0.97	4.62	77.40	14.41	8.19	1.82
SD	13.80	6.20	5.76	10.00	0.94	6.55	0.31	0.91	4.84	2.65	2.30	0.27
Rank	4	3	3	4	5	5	5	6	3	5	6	2
Mid-Metatarsal Shaft	20.38	14.85	14.11	5.52	5.33	48.68	1.18	7.42	72.46	17.52	10.02	1.97
SD	4.52	2.67	2.75	3.42	3.49	7.96	0.87	1.54	4.27	1.26	4.39	0.73
Rank	6	6	6	6	1	1	3	2	5	3	3	1
Rib	13.00	8.37	8.00	4.63	5.00	41.89	1.23	8.29	61.85	22.11	16.04	1.38
SD	3.57	1.04	1.13	2.94	1.93	6.48	0.50	2.06	5.49	3.64	2.27	0.15
Rank	7	7	7	7	2	2	2	1	6	2	2	6
Mean	**70.16**	**42.80**	**41.37**	**27.36**	**3.56**	**35.22**	**1.06**	**5.63**	**72.01**	**16.97**	**11.02**	**1.64**
SD	**44.46**	**21.17**	**20.46**	**27.88**	**1.90**	**9.70**	**0.52**	**1.81**	**7.92**	**4.08**	**4.15**	**0.37**

Table II.8 **DIFFERENCES BETWEEN ST. BERNARD AND BEAGLE IN CANCELLOUS BONE HISTOMORPHOMETRY**

Parameters	unit	St. Bernard	Beagle	% difference (Beagle/St. Bernard)
Trabecular area	%	18.67	22.17	19
Trabecular thickness	µm	110.07	95.27	-13
Trabecular number	#/mm	1.69	2.35	39
Trabecular separation	µm	715.61	482.14	-33
Ratio of surface to volume	mm/mm^2	16	18.3	14
Wall thickness	µm	50.55	42.96	-15
Labeled surface	%	8.99	8.2	-9
Mineral apposition rate	µm/d	1.07	0.77	-28
Mineralization lag time	day	10.54	13.83	31
Bone formation rate	%/yr	61.24	43.43	-29
Formation period	day	49.48	66.26	34

Table II.9 **DIFFERENCES BETWEEN ST. BERNARD AND BEAGLE IN CORTICAL BONE HISTOMORPHOMETRY**

Parameters	unit	St. Bernard	Beagle	% difference (Beagle/St. Bernard)
Total cross sectional area	mm^2	312.51	71.29	-77
Cortical area	mm^2	104.84	44.57	-57
Percent cortical area	%	38.71	66.01	71
Marrow area	mm^2	207.67	26.71	-87
Percent marrow area	%	61.29	33.99	-45
Percent porosity area	%	3.77	1.51	-60
Cortical bone area	mm^2	100.75	44.02	-56
Percent cortical bone area	%	37.5	65.12	74
Labeled osteonal surface	mm/mm^2	0.099	0.052	-47
Mineral apposition rate	µm/d	1.09	0.66	-40
Mineralization lag time	day	8.88	12.16	37
Bone formation rate	%/yr	4.02	1.46	-64
Formation period	day	56.34	87.92	56
Resorption period	day	16.55	31.67	91
Activation frequency	#/yr	2.4	1.68	-30

III. Adaptation of Cancellous and Cortical Bone to Immobilization and Overloading in the Rat.

Nine-month old female rats were subjected to right hindlimb immobilization or served as controls for 0, 2, 10, 18, and 26, weeks and were double-labeled with bone markers. The right limb was immobilized against the abdomen and considered unloaded, while the left limb was overloaded during ambulation. Changes in the continuously overloaded limb was compared to that in both limbs of the age-matched control animals.

1. In the unloaded limb, immobilization-induced muscle and cancellous bone loss occurred rapidly before 10 weeks and stabilized at 50% less bone mass after 18 weeks. Unloading caused a negative bone balance from a combination of elevated bone resorption and depressed bone formation. At 2, 10, and 18 weeks of immobilization, the ratios of bone resorption to bone formation surfaces were 1.6, 1.5, and 1.3, respectively; at 26 weeks, the ratio was 1. These observations indicate decreased mechanical usage, caused bone loss by stimulating bone turnover dependent bone loss. (Li, X.J., W.S.S. Jee, S.Y. Chow and D.M. Woodbury. Adaptation of cancellous bone to aging and immobilization in the rat: A single photon absorptiometry and histomorphometry study. Anat. Rec. 227:12-24).
2. In the overloaded limb, continuous overloading by 18 and 26 weeks induced increase cancellous bone mass. Our findings support the conclusions that increased mechanical usage caused a positive bone balance by depressing bone turnover dependent bone loss. (W.S.S. Jee and Li, X.J. Adaptation of cancellous bone to overloading in the adult rat: A single photon absorptiometry and histomorphometry study. Anat. Rec. [in press]).
3. Unloading accelerated age-related cortical bone loss by shutting off nearly all periosteal bone formation and slightly accelerating bone marrow expansion over that which occurs in age-related controls. Our results support the conclusions that decreased mechanical usage caused cortical bone loss by depression bone modeling dependent bone gain (by decreasing of modeling in the formation mode) and stimulating bone turnover dependent bone loss (by increasing activation frequency for remodeling that alters bone balance in favor of resorption at each site). (Li, X.J. and Jee, W.S.S. Adaptation of diaphyseal structure to aging and decreased mechanical loading in the adult rat. Anat. Rec. [submitted]).
4. Age-related loss is due to marrow cavity enlargement exceeding periosteal new bone formation. Overloading enhancing periosteal bone modeling in the formation mode and dampening endocortical bone remodeling to create a slight positive bone balance. These observations are in general agreement with the postulate that increased mechanical usage increased cortical bone mass by stimulating periosteal bone

modeling-dependent bone gain and depressing endosteal bone turnover (remodeling) dependent bone loss. (Jee, W.S.S., Li, X.J. and Schaffler, M.B. Adaptation of diaphyseal structure with aging and increased mechanical loading in the adult rat. Anat. Rec. [submitted]).

Importance: The present data on bone morphometry are fragmentary and unreliable. We have therefore generated static and dynamic morphometry data of multiple sites of cancellous and cortical bone that will allow us to reliably calculate bone cell residence time to ^{239}Pu- and ^{226}Ra-induced bone sarcoma sites.

The information on the impact of mechanical usage on cancellous and cortical bone mass and turnover rates will be used to improve our extrapolation of beagle data to people.

3) Task III: Microscopic Distribution of ^{239}Pu

In terminating the beagle colony in Salt Lake city, we were fortunate to have enough young adult beagles available to carry out "metabolic study for the determination of average and local dose rates, and bone parameter under initial conditions of temporary confinement and non-confinement. This project will provide detailed essential information for the construction of bone and soft tissue dosimetric-metabolic models. Fourteen young adult beagles were injected without prior confinement with 0.09 μCi Pu-239/kg and sacrificed sequentially between 1 to 64 weeks after injection. For comparison 15 additional beagles were confined for the usual 4 week period at injection. These dogs were sacrificed sequentially in groups of three between 4 weeks and 64 weeks after injection. Dogs received up to three treatment regimens with fluorescent bone markers for the evaluation of bone turnover rates as a function of temporary confinement and non-confinement. Detailed skeletal and soft tissue retention data and information on bone morphology and turnover rates will be collected. Together with earlier data obtained from 14 equally confined beagles (Wronski, Smith and Jee. The microdistribution and retention of injected 239Pu on trabecular bone surfaces of the beagle: Implications for the induction of osteosarcoma. Rad. Res. 83:74-89, 1980), this experiment will provide detailed information on the influence of confinement on the Pu distribution and the associated biological parameters, and on the dependency of Pu translocation on turnover activity. The resulting models will be the backbone of future dose response relationships for our Pu-toxicity study. The bone sites chosen for analysis were the fourth lumbar vertebral body, proximal ulna, proximal, distal, and mid humerus. Photographs of random sample sites of neutron-induced autoradiographs (W.S.S. Jee, R.B. Dell and L.G. Miller. High resolution neutron-induced autoradiographs of bone containing ^{239}Pu. Health Phys. 22:761-763, 1972) and fluorescent micrographs of the same areas were analyzed. The analytical program provide numerical information on 1) total Pu-239 content of selected areas of bone sections, 2) the anatomical location of Pu on surfaces, in bone mineral and bone marrow, and 3)

select bone morphometric parameters. The methodology for the microdistribution of Pu-239 are briefly summarized below.

1) A method to analyze neutron-induced autoradiographs (NIAR) from ^{239}Pu contaminated bone sections.

Thirty-five mm slides of randomly sampled sites of neutron-induced autoradiographs of bone sections were analyzed.The method requires a digitizing table and an appropriate computer for conversion of the visual image into a digital presentation of that image. Four output of that image other than screen display, a peripheral output device (line printer, laser printer, etc.) is required. Table and computer are under control of task oriented software. The flow of information is as follows:

Local Distribution of 239Pu Using Digitized Images of Neutron-Induced Autoradiographs

A procedure has been developed to determine quantitatively the local distribution of ^{239}Pu in bone from neutron-induced autoradiographs (NIARS). A number of frames, sufficient to provide statistically valid data, are randomly selected from the NIAR and photographed through a microscope. These photographs are projected onto a programmed digitizing tablet that is connected to a desktop computer. The image of the bone features and the fission tracks are traced manually and converted into their digitized representations. Tracks are assigned separately to bone volume, bone marrow and bone surfaces. Special track patterns such as lines of tracks representing Pu in buried initial surface deposits, diffuse tracks in "packets" of new bone with a visible track distribution, and clusters of Pu in marrow (stars) are traced as well. All numerical and pictorial information is accessible for further computer processing. An improved procedure to convert fission track densities to local Pu concentrations and to correct for fission tracks originating from slanted bone surfaces is presented. This method provides a reliable and statistically valid basis for the evaluation of all essential parameters necessary for local dosimetry. (Bruenger, F.W., Polig, E. and Jee, W.S.S. Local distribution of $2^{39}Pu$ using digitized images of neutron-induced autoradiographs. Radiation Protection Dosimetry (submitted).

Task IV. Calculation of Cell-specific Radiation Dosimetry

We have not neglected this part of our program which keeps us well focused. We have generated two articles for this task: one on bone parameters, dosimetry and radiation risk in the beagle skeleton and the other on alpha-emitting radionuclides hit rates to nuclei of bone-lining cells.

A variety of morphometric and histomorphometric parameters such as the mass of bone and marrow, bone surface areas, percentage of bone volume, percentage of the surface that is trabecular, and percentage of surfaces that are forming and resting are calculated for all major parts of the beagle skeleton. The total bone surface of the beagle is estimated at 1.9 m^2 with 53.7% of the surface area being associated with trabecular bone. There are about 4.5×10^9 osteoblasts. From the fractional retention in each part of the skeleton, the initial surface concentration of ^{239}Pu

after a single injection of 592 Bq/kg body wt (0.016 μCi/kg) on resting surfaces and at sites of bone formation is calculated for various values of the affinity ratios of trabecular/cortical and forming/resting surfaces. These estimated concentrations then yield dose rates as well as cumulative and collective doses to bone-lining cells and osteoblasts in the different parts of the skeleton.

On the assumption that the relative risk of tumor induction is proportional to the collective dose to either bone-lining cells or osteoblasts, the frequency of tumor occurrence is calculated and compared to observed frequencies. Both hypotheses yield approximate agreement with experimental data for different ratios of trabecular/cortical radiation sensitivity, although the differences between some bones are statistically significant. (Polig, E. and Jee, W.S.S. Bone structural parameters, dosimetry, and relative radiation risk in the beagle skeleton. Radiat. Res. 120:83-101, 1989).

Hit factors relating the local concentration of a bone-seeking α–emitter to the mean hit rate have been determined for nuclei of bone-lining cells using a Monte Carlo procedure. Cell nuclei were approximated by oblate spheroids with dimensions and location taken from a previous histomorphometric study. The Monte Carlo simulation is applicable for planar and diffuse labels at plane or cylindrical bone surfaces.

Our calculations show the existing standard for dose limitations implies that a large fraction of nuclei of cells lining bone surfaces are traversed by α-particles. This is of particular importance with regard to tumor induction, as the cell nucleus is believed to be the sensitive region, and α-particle traversal is the critical event. At present there is no unequivocal evidence for the lining cell to be the cell at risk, nor is it known how many traversals are required for an induction. The linear dose-effect relationship seen in beagle dogs contaminated with α-emitting transuranics and ^{226}Ra seems to imply that a single hit is sufficient (C.W. Mays et al., Cancer incidence and lifespan vs. α-particle dose in beagles. Health Phys. 52:617-625, 1987) whereas epidemiological analysis of human cases with radium body burdens suggests that two hits may be required (R.E. Rowland et al., Dose response relationships for female radium dial workers. Radiat. Res. 76:368-383, 1978). The above analysis also shows that the fraction of cells receiving exactly one hit is not much different for the two trabecular turnover rates considered here. (Polig, E. and Jee, W.S.S. Hit rates to nuclei of bone-lining cells from alpha-emitting radionuclides. Radiat. Res., submitted).
Importance: The first article emphasizes the need for more and better static and dynamic bone histomorphometry as well as microdistribution of 239Pu data. The latter article will enable us to calculate hit frequencies for the low and high incidence osteosarcoma bone sites and render support to whether one or two is sufficient for bone sarcoma induction.

END

DATE FILMED

12/03/90